Inorganic Chemistry

Bis(α-diimine)nickel Complexes: Molecular and Electronic Structure of Three Members of the Electron-Transfer Series [Ni(L)$_2$]^z (*z* = 0, 1+, 2+) (L = 2-Phenyl-1,4-bis(isopropyl)-1,4-diazabutadiene). A Combined Experimental and Theoretical Study

Nicoleta Muresan,[†] Krzysztof Chlopek,[‡] Thomas Weyhermüller,[†] Frank Neese,[§] and Karl Wieghardt*,[†]

Max-Planck-Institut für Bioanorganische Chemie, Stiftstrasse 34-36, D-45470 Mülheim an der Ruhr, Germany, Forschungszentrum Karlsruhe GmbH, Institut für Nanotechnologie, Postfach 3640, D-76021 Karlsruhe, Germany, and Institut für Physikalische und Theoretische Chemie, Wegelerstrasse 12, D-53115 Bonn, Germany

From the reaction of Ni(COD)$_2$ (COD = cyclooctadiene) in dry diethylether with 2 equiv of 2-phenyl-1,4-bis(isopropyl)-1,4-diazabutadiene (L^{Ox})^0 under an Ar atmosphere, dark red, diamagnetic microcrystals of [Ni^{II}(L$^•$)$_2$] (**1**) were obtained where (L$^•$)$^{1-}$ represents the π radical anion of neutral (L^{Ox})^0 and (L^{Red})$^{2-}$ is the closed shell, doubly reduced form of (L^{Ox})^0. Oxidation of **1** with 1 equiv of ferrocenium hexafluorophosphate in CH$_2$Cl$_2$ yields a paramagnetic ($S = 1/2$), dark violet precipitate of [Ni^I(L^{Ox})$_2$](PF$_6$) (**2**) which represents an oxidatively induced reduction of the central nickel ion. From the same reaction but with 2 equiv of [Fc](PF$_6$) in CH$_2$Cl$_2$, light green crystals of [Ni^{II}(L^{Ox})$_2$(FPF$_5$)](PF$_6$) (**3**) ($S = 1$) were obtained. If the same reaction was carried out in tetrahydrofuran, crystals of [Ni^{II}(L^{Ox})$_2$(THF)(FPF$_5$)](PF$_6$)·THF (**4**) ($S = 1$) were obtained. Compounds **1**, **2**, **3**, and **4** were structurally characterized by X-ray crystallography: **1** and **2** contain a tetrahedral neutral complex and a tetrahedral monocation, respectively, whereas **3** contains the five-coordinate cation [Ni^{II}(L^{Ox})$_2$(FPF$_5$)]$^+$ with a weakly coordinated PF$_6^-$ anion and in **4** the six-coordinate monocation [Ni^{II}(L^{Ox})$_2$(THF)(FPF$_5$)]$^+$ is present. The electro- and magnetochemistry of **1**–**4** has been investigated by cyclic voltammetry and SQUID measurements. UV–vis and EPR spectroscopic data for all compounds are reported. The experimental results have been confirmed by broken symmetry DFT calculations of [Ni^{II}(L$^•$)$_2$]^0, [Ni^I(L^{Ox})$_2$]$^+$, and [Ni^{II}(L^{Ox})$_2$]$^{2+}$ in comparison with calculations of the corresponding Zn complexes: [Zn^{II}(^{t}L^{Ox})$_2$]$^{2+}$, [Zn^{II}(^{t}L^{Ox})(^{t}L$^•$)]$^+$, [Zn^{II}(^{t}L$^•$)$_2$]^0, and [Zn^{II}(^{t}L$^•$)(^{t}L^{Red})]$^-$ where (^{t}L^{Ox})^0 represents the neutral ligand 1,4-di-*tert*-butyl-1,4-diaza-1,3-butadiene and (^{t}L$^•$)$^{1-}$ and (^{t}L^{Red})$^{2-}$ are the corresponding one- and two-electron reduced forms. It is clearly established that the electronic structures of both paramagnetic monocations [Ni^I(L^{Ox})$_2$]$^+$ ($S = 1/2$) and [Zn^{II}(^{t}L^{Ox})(^{t}L$^•$)]$^+$ ($S = 1/2$) are different.

Introduction

The coordination chemistry of N,N′-disubstituted α-diimines with main group metal ions (Li, Mg, Al, Ga, In) has been investigated in detail in the past.[1–12] It has been discovered mainly by X-ray crystallography that these ligands can adopt three different oxidation levels, namely the neutral

* To whom correspondence should be addressed. E-mail: wieghardt@ mpi-muelheim.mpg.de. Phone: ++49-208-306 3610. Fax: ++49-208-306 3952.
† Max-Planck-Institut für Bioanorganische Chemie.
‡ Institut für Nanotechnologie.
§ Institut für Physikalische und Theoretische Chemie.

 (1) van Koten, G.; Vrieze, K. *Adv. Organomet. Chem.* **1982**, *21*, 151.
 (2) Richter, S.; Daul, C.; von Zelewsky, A. *Inorg. Chem.* **1976**, *15*, 943.
 (3) Corvaja, C.; Pasimeni, L. *Chem. Phys. Lett.* **1976**, 261.
 (4) Cloke, F. G. N.; Hanson, G. R.; Henderson, M. J.; Hitchcock, P. B.; Raston, C. L. *J. Chem. Soc., Chem. Commun.* **1989**, 100.
 (5) Cloke, F. G. N.; Dalby, C. I.; Henderson, M. J.; Hitchcock, P. B.; Kennard, C. H. L.; Lamb, R. N.; Raston, C. L. *J. Chem. Soc., Chem. Commun.* **1990**, 1394.
 (6) Thiele, K.-H.; Lorenz, V.; Thiele, G.; Zönnchen, P.; Scholz, J. *Angew. Chem., Int. Ed. Engl.* **1994**, *33*, 1372.
 (7) Gardiner, M. G.; Hanson, G. R.; Henderson, M. J.; Lee, F. C.; Raston, C. L. *Inorg. Chem.* **1994**, *33*, 2456.
 (8) Rijnberg, E.; Richter, B.; Thiele, K.-H.; Boersma, J.; Veldman, N.; Spek, A. L.; van Koten, G. *Inorg. Chem.* **1998**, *37*, 56.
 (9) Pott, T.; Jutzi, P.; Neumann, B.; Stammler, H.-G. *Organometallics* **2001**, *20*, 1965.

Scheme 1. Ligands and Abbreviations[a]
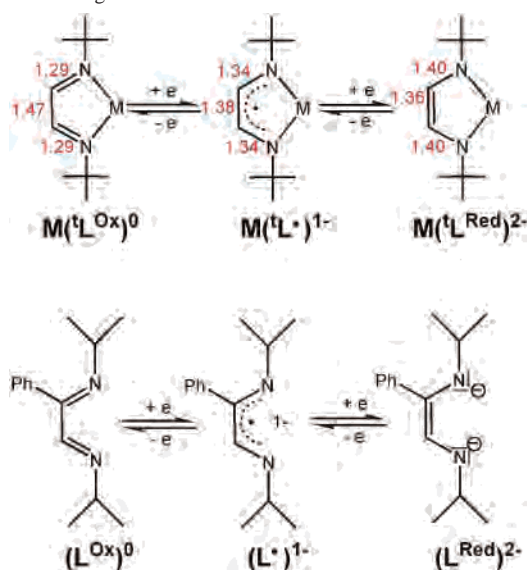
[a] Red numbers represent av bond lengths in Å.

α-diimines $(L^{Ox})^0$, monoanionic π radicals $(L^{\bullet})^{1-}$, and reduced dianionic α-diamides $(L^{Red})^{2-}$ as shown in Scheme 1. Interestingly, X-ray crystallography has unambiguously demonstrated that the three ligand oxidation levels can be identified by their varying C—N and C—C bond lengths: for $(L^{Ox})^0$ the average C—N and C—C bond distances are at 1.29 ± 0.01 and 1.47 ± 0.01 Å, respectively, whereas those for the π radical monoanions are at 1.34 ± 0.01 and 1.38 ± 0.01 Å, and finally, those in the dianions are at 1.40 ± 0.01 and 1.36 ± 0.01 Å (Scheme 1).

Raston et al.[7] and van Koten et al.[8] have synthesized and structurally characterized the following members of an electron-transfer series: $K_2[Zn^{II}({}^tL^{Red})_2]$, $K[Zn^{II}({}^tL^{Red})({}^tL^{\bullet})]$, $[Zn^{II}({}^tL^{\bullet})_2]$, $[Zn^{II}({}^tL^{Ox})({}^tL^{\bullet})](OTf)$, $[Zn^{II}({}^tL^{Ox})_2](OTf)_2$ where $({}^tL^{Ox})^0$, $({}^tL^{\bullet})^{1-}$, and $({}^tL^{Red})^{2-}$ represent the three oxidation levels of 1,4-di-*tert*-butyl-1,4-diaza-1,3-butadiene. The most important observations are that the ZnN_4 polyhedron is in all cases tetrahedral and that in the two paramagnetic species, namely the monoanion and the monocation, respectively, the two ligands exist in differing oxidation levels, which is clearly borne out by the observed structural parameters. Thus, the unpaired electron is localized on one monoanionic $({}^tL^{\bullet})^{1-}$ ligand; no delocalization of this electron over both ligands is observed. The same is true for tetrahedral, paramagnetic complexes $[M^{III}(L^{Red})(L^{\bullet})]^0$ (M = Al, Ga).[1–12]

Recent DFT calculations on these latter complexes have reliably reproduced these structures.[13,14] The calculated and experimental EPR parameters agree nicely, giving confidence that the unpaired electron resides in a π* ligand orbital of

the $(L^{\bullet})^{1-}$ ligand. It is therefore quite surprising that despite our above apparently clear understanding of the molecular and electronic structures of the main group metal (and Zn^{II}) complexes this was until very recently not the case for similar transition metal complexes of α-diimines. Thus, all neutral, tetrahedral, and diamagnetic bis(α-diimine)metal complexes of Ni (and paramagnetic Fe) have been described as Ni(0) $(d^{10})^{15–20}$ or Fe(0) $(d^8)^{21–23}$ complexes containing two neutral, diamagnetic α-diimine ligands (L^{Ox}). We[24,25] and others[26] have shown recently for the first time that the nickel complexes contain in fact a central Ni(II) ion with a high spin d^8 electron configuration $(S_{Ni} = 1)$ which is coupled intramolecularly antiferromagnetically to two ligand π radicals $(L^{\bullet})^{1-}$ $(S_{rad} = {}^1/_2)$: their electronic structures are thus best described as $[Ni^{II}(L^{\bullet})_2]$ $(S_t = 0)$ and *not* $[Ni^0(L^{Ox})_2]$ $(S_t = 0)$.

It is an interesting observation that these neutral complexes $[Ni^{II}(L^{\bullet})_2]$ can be reversibly twice oxidized yielding a mono- and a dication and, in some cases, also twice reduced affording a mono- and dianion, respectively. Thus, these complexes are members of an electron-transfer series.[15] The molecular and electronic structures of these ionic members have not been studied in the past. Here we report the syntheses and characterization of the three-membered series: $[Ni^{II}(L^{\bullet})_2]^0$, $[Ni^{II}(L^{\bullet})(L^{Ox})]^+$, and $[Ni^{II}(L^{Ox})_2]^{2+}$ where $(L^{Ox})^0$, $(L^{\bullet})^{1-}$, and $(L^{Red})^{2-}$ represent the redox members of the asymmetric α-diimine ligand 2-phenyl-1,4-bis(isopropyl)-1,4-diaza-1,3-butadiene (Schemes 1 and 2).

We establish their molecular and electronic structures experimentally and also by density functional theoretical (DFT) calculations. In order to calibrate this methodology for the three nickel complexes **1**, **2**, and **3** (Scheme 2), we have also calculated and optimized the geometry of the corresponding Zn complexes from refs 2, 7, and 8.
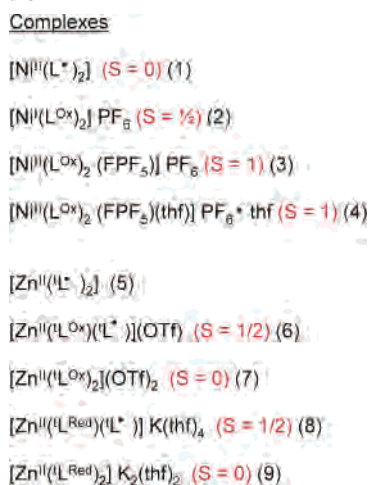
Experimental Section

All air-sensitive materials were manipulated under argon using standard Schlenk line procedures or a glovebox. Bis(cyclooctadiene)nickel(0) and ferrocenium hexafluorophosphate were purchased from Aldrich. All chemicals were used without further purification.

(10) Baker, R. J.; Farley, R. D.; Jones, C.; Mills, D. P.; Kloth, M.; Murphy, D. M. *Chem.—Eur. J.* **2005**, *11*, 2972.
(11) Pott, T.; Jutzi, P.; Kaim, W.; Schoeller, W. W.; Neumann, B.; Stammler, A.; Stammler, H.-G.; Wanner, M. *Organometallics* **2002**, *21*, 3169.
(12) (a) Baker, R. J.; Farley, R. D.; Jones, C.; Kloth, M.; Murphy, D. M. *Chem. Commun.* **2002**, 1196. (b) Baker, R. J.; Farley, R. D.; Jones, C.; Kloth, M.; Murphy, D. M. *Dalton Trans.* **2002**, 3844.
(13) Tuononen, H. M.; Armstrong, A. F. *Dalton Trans.* **2006**, 1885.
(14) Tuononen, H. M.; Armstrong, A. F. *Inorg. Chem.* **2005**, *44*, 8277.
(15) Baloh, A. L.; Holm, R. H. *J. Am. Chem. Soc.* **1966**, *88*, 5201.
(16) tom Dieck, H.; Svoboda, M.; Kopf, J. *Z. Naturforsch., B: Chem. Sci.* **1978**, *33*, 1381.
(17) Walther, D. *Z. Anorg. Allg. Chem.* **1974**, *405*, 8.
(18) (a) Svoboda, M.; tom Dieck, H. *Z. Naturforsch., B: Chem. Sci.* **1981**, *36*, 814. (b) tom Dieck, H.; Svoboda, M.; Greiser, T. *Z. Naturforsch., B: Chem. Sci.* **1981**, *36*, 823.
(19) Görls, H.; Walther, D.; Siedler, J. *Cryst. Res. Technol.* **1987**, *22*, 1145.
(20) Bonrath, W.; Pörschke, K. R.; Mynott, R.; Krüger, C. *Z. Naturforsch., B: Chem. Sci.* **1990**, *45*, 1647.
(21) tom Dieck, H.; Bruder, H. *J. Chem. Soc., Chem. Commun.* **1977**, 24.
(22) Walther, D.; Kreisel, G.; Kirmse, R. *Z. Anorg. Allg. Chem.* **1982**, *487*, 149.
(23) Bart, S. C.; Hawrelak, E. J.; Lobkovsky, E.; Chirik, P. *Organometallics* **2005**, *24*, 5518.
(24) Blanchard, S.; Neese, F.; Bothe, E.; Bill, E.; Weyhermüller, T.; Wieghardt, K. *Inorg. Chem.* **2005**, *44*, 3636.
(25) Chlopek, K.; Bothe, E.; Neese, F.; Weyhermüller, T.; Wieghardt, K. *Inorg. Chem.* **2006**, *45*, 6298.
(26) Khusniyarov, M. M.; Harms, K.; Burghaus, O.; Sundermeyer, J. *Eur. J. Inorg. Chem.* **2006**, *15*, 2985.

Scheme 2. New Complexes of Nickel and Zinc Complexes from References 7 and 8

Complexes

$[Ni^{II}(L^{\bullet})_2]$ (S = 0) (1)

$[Ni^{I}(L^{Ox})_2]$ PF$_6$ (S = ½) (2)

$[Ni^{II}(L^{Ox})_2$ (FPF$_5$)] PF$_6$ (S = 1) (3)

$[Ni^{II}(L^{Ox})_2$ (FPF$_5$)(thf)] PF$_6 \cdot$ thf (S = 1) (4)

$[Zn^{II}(L^{\bullet})_2]$ (5)

$[Zn^{II}(L^{Ox})(L^{\bullet})](OTf)$ (S = 1/2) (6)

$[Zn^{II}(L^{Ox})_2](OTf)_2$ (S = 0) (7)

$[Zn^{II}(L^{Red})(L^{\bullet})] K(thf)_4$ (S = 1/2) (8)

$[Zn^{II}(L^{Red})_2] K_2(thf)_2$ (S = 0) (9)

The ligand 2-phenyl-1,4-bis(isopropyl)-1,4-diazabutadiene was synthesized according to published procedures.[27]

$[Ni^{II}(L^{\bullet})_2]$ (1). To a solution of Ni(COD)$_2$ (1 g, 3.63 mmol) (COD = cyclooctadiene) in diethyl ether (20 mL) under an argon blanketing atmosphere was added a solution of 2-phenyl-1,4-bis-(isopropyl)-1,4-diazabutadiene (1.58 g, 7.27 mmol) in diethyl ether (10 mL). The reaction mixture was stirred overnight at room temperature. The color of the solution changed from yellow to deep red. The solvent was removed by evaporation under reduced pressure to give a dark red precipitate which was washed with acetonitrile and dried in vacuo. Yield: 1.40 g (78%). X-ray quality crystals were obtained by slow evaporation of the solvent from a concentrated solution of **1** in acetonitrile. Anal. Calcd for C$_{28}$H$_{40}$N$_4$Ni: C, 68.47; H, 8.15; N, 11.41; Ni, 11.97. Found: C, 68.31; H, 8.21; N, 11.64; Ni, 11.22.

^{1}H NMR (400 MHz, toluene-d_8): δ (ppm) = 1.75 (d, ^3J = 6.31, 6H, iPr-CH_3), 1.91 (d, ^3J = 6.49, 6H, iPr-CH_3), 1.89 (d, ^3J = 6.31, 6H, iPr-CH_3), 1.90 (d, ^3J = 6.49, 6H, iPr-CH_3), 2.65 (sept, ^3J = 6.49, 2H, iPr-CH), 3.66 (sept, ^3J = 6.31, 2H, iPr-CH), 6.9 (m, 4H, C$_6H_5$), 7.05 (m, 4H, C$_6H_5$), 7.16 (m, 2H, C$_6H_5$), 8.75 (s, 2H, NCH).

$[Ni^I(L^{Ox})_2]$ PF$_6$ (2). To a solution of **1** (200 mg, 0.40 mmol) in CH$_2$Cl$_2$ (10 mL) was added ferrocenium hexafluorophosphate (130 mg, 0.40 mmol) with stirring for 1.5 h at 20 °C. The dark red color of the solution immediately turned to dark violet. The resulting solution was filtered, and the filtrate was concentrated to ~1 mL by evaporation of the solvent under reduced pressure. *n*-Hexane (10 mL) was added, and the resulting suspension was stirred for 1 h. A dark violet precipitate was formed, washed with *n*-hexane (2 × 5 mL), and dried in vacuo. Yield: 0.20 g (80%). X-ray quality crystals were obtained by slow diffusion of n-pentane into a concentrated solution of **2** in THF. MS (ESI, pos ion, CH$_2$Cl$_2$), m/z = 490 {**2** − PF$_6$}$^+$. Anal. Calcd for C$_{28}$H$_{40}$N$_4$F$_6$NiP: C, 52.5; H, 6.29; N, 8.8; F, 17.93; Ni, 9.23; P, 4.87. Found: C, 52.76; H, 6.24; N, 8.89; F, 17.83; Ni, 9.37; P, 4.76.

$[Ni^{II}(L^{Ox})_2(FPF_5)](PF_6)$ (3). To a solution of **1** (300 mg, 0.61 mmol) in CH$_2$Cl$_2$ (10 mL) was added ferrocenium hexafluorophosphate (400 mg, 1.22 mmol) with stirring for 1.5 h at 20 °C. The dark red color of the solution immediately turned to light green. The resulting solution was filtered, and the filtrate was concentrated to ~1 mL by evaporation of the solvent under reduced pressure. *n*-Hexane (10 mL) was added, and the resulting suspension was

stirred for 1 h. A light green precipitate formed which was washed with *n*-hexane (2 × 5 mL) and dried in vacuo. Yield: 0.20 g (80%). X-ray quality crystals were obtained by slow diffusion of n-pentane into a concentrated solution of **3** in CH$_2$Cl$_2$. Anal. Calcd for C$_{28}$H$_{40}$N$_4$F$_{12}$NiP$_2$: C, 43.04; H, 5.12; N, 7.17; Ni, 7.51; P, 7.84. Found: C, 43.01; H, 5.46; N, 6.95; Ni, 7.25; P, 7.54.

$[Ni^{II}(L^{Ox})_2(THF)(FPF_5)](PF_6) \cdot THF$ (4). To a solution of **1** (200 mg, 0.4 mmol) in THF (10 mL) was added ferrocenium hexafluorophosphate (260 mg, 0.8 mmol) with stirring for 1.5 h at 20 °C. The dark red color of the solution immediately turned to light green. The resulting solution was filtered, and the filtrate was concentrated to ~1 mL by evaporation of the solvent under reduced pressure. *n*-Hexane (10 mL) was added, and the resulting suspension was stirred for 1 h. A slightly green precipitate was formed, washed with *n*-hexane, and dried in vacuo. Yield: 0.15 g (80%). X-ray quality crystals were obtained by slow diffusion of n-pentane into a concentrated solution of **4** in THF. Anal. Calcd for C$_{36}$H$_{56}$N$_4$F$_{12}$NiO$_2$P$_2$: C, 47.72; H, 6.10; N, 6.05. Found: C, 47.55; H, 6.08; N, 5.82.

X-ray Crystallographic Data Collection and Refinement of the Structures. A dark red single crystal of **1**, a dark blue crystal of **2**, and greenish yellow crystals of **3** and **4**·THF were coated with perfluoropolyether, picked up with nylon loops, and mounted in the nitrogen cold stream of the diffractometer. A Bruker-Nonius Kappa-CCD diffractometer equipped with a Mo-target rotating-anode X-ray source and a graphite monochromator (Mo Kα, λ = 0.71073 Å) was used. Final cell constants were obtained from least-squares fits of all measured reflections. Intensity data of **2**, **3**, and **4** were corrected for absorption using intensities of redundant reflections.

The structures were readily solved by direct methods and subsequent difference Fourier techniques. The Siemens ShelXTL[28] software package was used for solution and artwork of the structure; ShelXL97[29] was used for the refinement. All non-hydrogen atoms were refined anisotropically, except for a disordered tetrahydrofuran solvent molecule in **4** which was split on three positions and isotropically refined. Hydrogen atoms were placed at calculated positions and refined as riding atoms with isotropic displacement parameters. Crystallographic data of the compounds are listed in Table 1.

Disorder was found in all four structures. The asymmetric unit in **1** contains two crystallographically independent molecules of which the one containing Ni(1) had disordered isopropyl groups which were split on two positions in a 56:44 and 73:27 ratio, respectively. Corresponding atoms were restrained to have the same distances and thermal displacement parameters. The structure of **2** was fully refined in the enantiomorphic space groups P3$_1$21 (No. 152) and P3$_2$21 (No. 154). The R-factor and Flack[30] parameters were slightly lower for the solution in P3$_1$2$_1$, and therefore, this space group was chosen. The PF$_6^-$ anion lying on a crystallographic 2-fold axis was found to be disordered and was split on two positions in a 69:31 ratio. The P−F and F−F distances were restrained to be equal within errors, and equivalent thermal displacement parameters were used for neighboring split atoms. Similar problems occurred in the structure of **3** in which the isopropyl group attached to N(24), and the uncoordinated PF$_6^-$ anion was split in a 91:9 ratio. A total of 25 restraints was used to equal distances and displacement parameters using EADP, SADI,

(27) Armesto, D.; Bosch, P.; Gallego, M. G.; Martin, J. F.; Ortiz, M. J.; Perez-Ossorio, R.; Ramos, A. *Org. Prep. Proced. Int.* **1987**, *19*, 181.

(28) *ShelXTL V.5*; Siemens Analytical X-Ray Inst. Inc.: Madison, WI, 1994.

(29) Sheldrick, G. M. *ShelXL97*; University of Göttingen: Göttingen, Germany, 1997.

(30) (a) Flack, H. D. *Acta Crystallogr.* **1983**, *A39*, 876−881. (b) Bernadelli, G.; Glack, H. D. *Acta Crystallogr.* **1985**, *A41*, 500−511.

Table 1. Crystallographic Data for **1**, **2**, **3**, and **4·THF**

	1	**2**	**3**	**4·THF**
chem formula	$C_{28}H_{40}N_4Ni$	$C_{28}H_{40}F_6N_4NiP$	$C_{28}H_{40}F_{12}N_4NiP_2$	$C_{36}H_{56}F_{12}N_4NiO_2P_2$
fw	491.35	636.32	781.29	925.50
space group	$P\bar{1}$, No. 2	$P3_121$, No. 152	$P2_1/c$, No. 14	$P2_1/n$, No. 14
a, Å	10.1190(4)	9.1845(3)	18.8774(5)	12.5937(4)
b, Å	9.9954(3)	9.1845(3)	9.7865(2)	19.4208(6)
c, Å	26.5990(8)	30.6806(12)	18.6485(5)	18.1200(6)
α, deg	91.161(5)	90	90	90
β, deg	90.020(5)	90	106.408(3)	109.208(5)
γ, deg	99.519(5)	120	90	90
V, Å	2652.7(2)	2241.33(14)	3304.88(14)	4185.1(2)
Z	4	3	4	4
T, K	100(2)	100(2)	100(2)	100(2)
ρ calcd, g cm^{-3}	1.230	1.414	1.570	1.469
reflns collected/$2\Theta_{max}$	41996/52.00	25078/65.00	84831/60.00	74161/60.00
unique reflns/$I > 2\sigma(I)$	10392/7730	5405/4818	9630/7136	12180/9675
no. params/restraints	615/40	197/30	461/25	566/63
λ, Å/μ(Kα), cm^{-1}	0.71073/7.53	0.71073/7.65	0.71073/7.79	0.71073/6.31
R1^a/GOF^b	0.0504/1.058	0.0536/1.081	0.0418/1.018	0.0640/1.073
wR2^c ($I > 2\sigma(I)$)	0.0861	0.1197	0.0845	0.1540
residual density, e Å^{-3}	+0.49/−0.41	+0.89/−0.70	+0.73/−0.50	+1.18/−0.67

^{a} Observation criterion: $I > 2\sigma(I)$. R1 $= \sum||F_o| - |F_c||/\sum|F_o|$. ^{b} GOF $= [\sum[w(F_o^2 - F_c^2)^2]/(n - p)]^{1/2}$. ^{c} wR2 $= [\sum[w(F_o^2 - F_c^2)^2]/\sum[w(F_o^2)^2]]^{1/2}$ where $w = 1/\sigma^2(F_o^2) + (aP)^2 + bP$, $P = (F_o^2 + 2F_c^2)/3$.

and SAME instructions of ShelXL. Compound **4** showed disorder of the uncoordinated PF_6^- anion and both the coordinated and uncoordinated THF molecules. The PF_6^- split positions were refined with above-mentioned restraints from which a 84:16 ratio resulted. The coordinated THF was refined with a split ratio of 73:27, and the uncoordinated one was split on three positions (41:33:26) using EADP and SAME restraints (63 restraints).

Physical Measurements. Electronic spectra of complexes in CH_2Cl_2 solution and corresponding spectra from electrochemical measurements were recorded on an HP 8452A diode array spectrophotometer (range 200−1000 nm) or a Perkin-Elmer double-beam photometer (range 200−2000 nm). Cyclic voltammograms and coulometric experiments were performed with an EG&G potentiostat/galvanostat, model 273A. Variable field (1.0 T), variable temperature (4−300 K) magnetization data were recorded on a SQUID magnetometer (MPMS Quantum Design). The experimental magnetic susceptibility data were corrected for underlying diamagnetism by use of tabulated Pascal constants.

X-band EPR spectra were recorded on a Bruker ESP 300 spectrometer.

Calculations. All calculations were performed by using the ORCA program package.[31] The geometry optimizations were carried out at the B3LYP level[32] of DFT. The all-electron Gaussian basis sets were those reported by the Ahlrichs group.[33,34] Triple-ζ quality basis sets with one set of polarization functions on the nickel and nitrogen atoms were used (TZVP).[34] The carbon and hydrogen atoms were described by slightly smaller polarized split-valence SV(P) basis sets that are double-ζ quality in the valence region and contain a polarizing set of d-functions on the non-hydrogen atoms.[33] The auxiliary basis sets for all complexes used to expand the electron density in the calculations were chosen to match the orbital basis. The SCF calculations were tightly converged (1 × 10^{-8} Eh in energy, 1 × 10^{-7} Eh in the density change, and 1 ×

10^{-7} in the maximum element of the DIIS error vector). The geometries were considered converged after the energy change was less than 5 × 10^{-6} Eh, the gradient norm and maximum gradient element were smaller than 1 × 10^{-4} Eh/Bohr and 3 × 10^{-4} Eh/Bohr, respectively, and the root-mean square and maximum displacements of atoms were smaller than 2 × 10^{-3} Bohr and 4 × 10^{-3} Bohr, respectively. The starting geometries were those of the crystal structures of **1**, **2**, and **3** and those for the Zn complexes from ref 8. Corresponding orbitals[35] and density plots were obtained by the program Molekel.[36]

We describe our computational results of nickel and zinc complexes containing noninnocent ligands using the broken symmetry (BS) approach first proposed by Ginsberg[37] and standardized by Noodleman.[38,39] The BS approach has been successfully applied for transition-metal-containing complexes in the past in the groups of Wieghardt, Neese,[40−44] and others.[38,45]

Since for some of the complexes studied in this work one can obtain broken-symmetry (BS) solutions to the spin-unrestricted

(31) Neese, F. In *ORCA, an Ab Initio, Density Functional and Semiempirical Electronic Structure Program Package, Version 2.4, Revision 36*; Max-Planck Institut für Bioanorganische Chemie: Mülheim/Ruhr, Germany, May 2005.

(32) (a) Becke, A. D. *J. Chem. Phys.* **1993**, *98*, 5648. (b) Becke, A. D. *J. Chem. Phys.* **1986**, *84*, 4524. (c) Lee, C. T.; Yang, W. T.; Parr, R. G. *Phys. Rev. B* **1988**, *37*, 785.

(33) Schäfer, A.; Horn, H.; Ahlrichs, R. *J. Chem. Phys.* **1992**, *97*, 2571.

(34) Schäfer, A.; Huber, C.; Ahlrichs, R. *J. Chem. Phys.* **1994**, *100*, 5829.

(35) Neese, F. *J. Phys. Chem. Solids* **2004**, *65*, 781.

(36) Molekel. *Molekel, Advanced Interactive 3d-Graphics for Molecular Sciences*; available at http://www.cscs.ch/molekel/.

(37) Ginsberg, A. P. *J. Am. Chem. Soc.* **1980**, *102*, 111.

(38) Noodleman, L.; Peng, C. Y.; Case, D. A.; Mouesca, J. M. *Coord. Chem. Rev.* **1995**, *144*, 199.

(39) (a) Noodleman, L.; Case, D. A.; Aizman, A. *J. Am. Chem. Soc.* **1988**, *110*, 1001. (b) Noodleman, L.; Davidson, E. R. *Chem. Phys.* **1986**, *109*, 131. (c) Noodleman, L.; Norman, J. G.; Osborne, J. H.; Aizman, C.; Case, D. A. *J. Am. Chem. Soc.* **1985**, *107*, 3418. (d) Noodleman, L. *J. Chem. Phys.* **1981**, *74*, 5737.

(40) (a) Bachler, V.; Olbrich, G.; Neese, F.; Wieghardt, K. *Inorg. Chem.* **2002**, *41*, 4179. (b) Ghosh, P.; Bill, E.; Weyhermüller, T.; Neese, F.; Wieghardt, K. *J. Am. Chem. Soc.* **2003**, *125*, 1293.

(41) (a) Herebian, D.; Bothe, E.; Neese, F.; Weyhermüller, T.; Wieghardt, K. *J. Am. Chem. Soc.* **2003**, *125*, 9116. (b) Herebian, D.; Wieghardt, K.; Neese, F. *J. Am. Chem. Soc.* **2003**, *125*, 10997.

(42) Slep, L. D.; Mijovilovich, A.; Meyer-Klaucke, W.; Weyhermüller, T.; Bill, E.; Bothe, E.; Neese, F.; Wieghardt, K. *J. Am. Chem. Soc.* **2003**, *125*, 15554.

(43) Chlopek, K.; Bothe, E.; Neese, F.; Weyhermüller, T.; Wieghardt, K. *Inorg. Chem.* **2006**, *45*, 6298.

(44) Patra, A. K.; Bill, E.; Bothe, E.; Chlopek, K.; Neese, F.; Weyhermüller, T.; Stobie, K.; Ward, M. D.; McCleverty, J. A.; Wieghardt, K. *Inorg. Chem.* **2006**, *45*, 7877.

(45) (a) Remenyi, C.; Kaupp, M. *J. Am. Chem. Soc.* **2005**, *127*, 11399. (b) Bencini, A.; Carbonera, C.; Dei, A.; Vaz, M. G. F. *Dalton Trans.* **2003**, 1701.

Table 2. Selected Bond Lengths (Å) in **1**, **2**, **3**, and **4**

	1				2	3		4	
Ni1−N1	1.940(2)[a]	1.938(2)[a]	1.932(2)[b]	1.936(2)[b]	1.987(2)	2.032(2)	1.993(2)	2.084(3)	2.095(2)
Ni1−N4	1.924(2)	1.934(2)	1.914(3)	1.917(3)	1.979(2)	2.013(2)	1.997(2)	2.043(2)	2.044(2)
N1−C2	1.338(3)	1.336(3)	1.333(4)	1.338(4)	1.305(3)	1.291(3)	1.293(2)	1.289(4)	1.292(3)
C2−C3	1.409(4)	1.418(4)	1.420(4)	1.411(4)	1.461(3)	1.499(3)	1.496(3)	1.496(4)	1.490(4)
C3−N4	1.322(4)	1.313(3)	1.322(4)	1.319(4)	1.294(3)	1.266(3)	1.272(2)	1.267(4)	1.262(4)
θ, deg[c]	78.9(3)		78.4(2)		70.0(2)	86.6			

[a] Molecule 1 with two ligands (L•)$^{1-}$. [b] Molecule 2 with two (L•)$^{1-}$ ligands. [c] Dihedral angle between two metallacycles Ni−N−C−C−N.
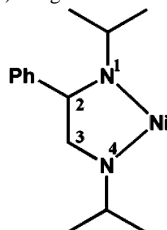
Kohn−Sham equations, we will adopt the following notation: the given system (molecule, ion) is divided into two fragments. The notation BS(m,n) then refers to a broken symmetry state with m unpaired spin-up electrons on fragment 1 and n unpaired spin-down electrons essentially localized on fragment 2. In most cases, fragments 1 and 2 correspond to the metal and the ligand, respectively. Note that in this notation a standard high-spin open-shell solution would be written down as BS($m+n$,0). In general, the BS(m,n) notation refers to the initial guess to the wavefunction. The variational process does, however, have the freedom to converge to a solution of the form BS($m−n$,0) where effectively the n-spin-down electrons pair with $n < m$ spin-up electrons on the partner fragment. Such a solution is then a standard $M_s \cong S = (m − n)/2$ unrestricted Kohn−Sham solution. As explained elsewhere,[35] the nature of the solution is investigated via the corresponding orbital transformation which via the corresponding orbital overlaps displays whether the system is to be described as a spin-coupled or a closed-shell solution.

Results

1. Synthesis and Characterization of Complexes. The reaction of Ni(COD)$_2$ (COD = cyclooctadiene) at 20 °C with 2 equiv of 2-phenyl-1,4-bis(isopropyl)-1,4-diazabutadiene,[27] (L^{Ox})^0, in diethyl ether under an Ar blanketing atmosphere affords dark red microcrystals of [Ni^{II}(L•)$_2$] (**1**) in 78% yield after evaporation of the solvent. As judged from its normal ^{1}H NMR spectrum (see Experimental Section), **1** is diamagnetic with an $S = 0$ ground state.

Complex **1** was oxidized by 1 equiv of ferrocenium hexafluorophosphate in CH$_2$Cl$_2$ solution yielding a dark violet precipitate of [Ni^I(L^{Ox})$_2$](PF$_6$) (**2**) after evaporation of the solvent and addition of n-hexane. From variable temperature (4−300 K) magnetic susceptibility measurements (SQUID) a temperature-independent magnetic moment of 2.1 μ_B was established for a solid sample of **2**. Thus, **2** possesses an $S = \frac{1}{2}$ ground state.

If 2 equiv of ferrocenium hexafluorophosphate was employed in the above reaction, a light green precipitate of [Ni^{II}(L^{Ox})$_2$(FPF$_5$)](PF$_6$) (**3**) was obtained in 80% yield. Variable temperature magnetic susceptibility measurements exhibit a temperature-independent magnetic moment of 3.2 μ_B (10−300 K) indicating an $S = 1$ ground state for **3**.

Recrystallization of **3** from dry tetrahydrofuran solution affords light green crystals of [Ni^{II}(L^{Ox})$_2$(FPF$_5$)(THF)](PF$_6$)• THF (**4**) which are again paramagnetic ($\mu = 3.1$ μ_B (10− 300 K); $S = 1$).

2. Crystal Structure Determinations. The crystal structures of **1**, **2**, **3**, and **4** have been determined at 100(2) K. Table 1 summarizes the crystallographic details, and Table 2 gives selected bond distances of the five-membered chelate rings Ni−N−C−C−N. Figure 1 displays a single neutral molecule in crystals of **1**, Figure 2 exhibits an ion pair in crystals of **2**, and Figure 3 shows that of a [Ni^I(L^{Ox})$_2$(FPF$_5$)]$^+$ monocation in crystals of **3**, whereas in Figure 4 the monocation [Ni^{II}(L^{Ox})$_2$(THF)(FPF$_5$)]$^+$ in **4** is shown.
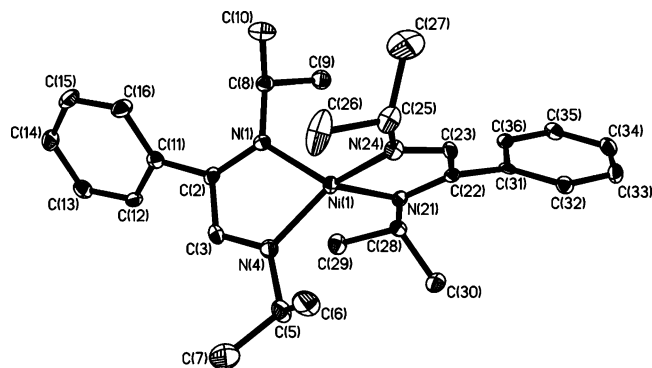
Figure 1. Structure of one of the two crystallographically independent neutral molecules in crystals of **1** (ellipsoids are drawn at the 50% probability level).
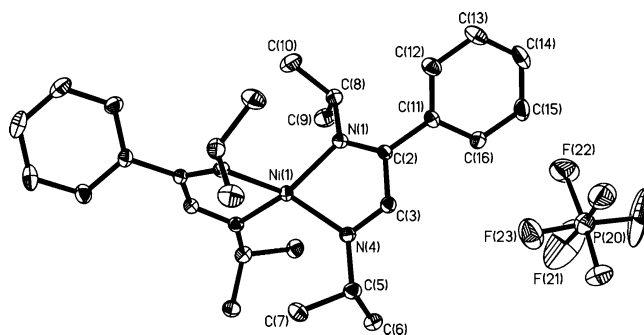
Figure 2. Structures of the monocation and the corresponding well-separated PF$_6$ anion in crystals of **2** (ellipsoids at the 50% probability level).
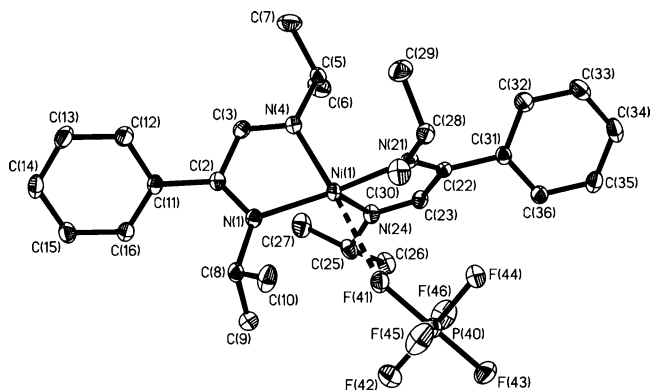
Figure 3. Structure of the five-coordinate monocation $[Ni^{II}(L^{Ox})_2(FPF_5)]^+$ in crystals of **3** (ellipsoids are at the 50% probability level).
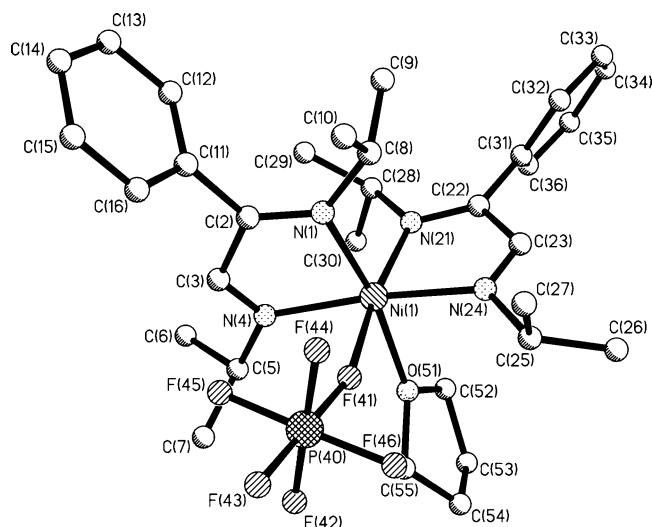

Figure 4. Structure of the six-coordinate monocation $[Ni^{II}(L^{Ox})_2(THF)-(FPF_5)]^+$ in crystals of **4**.

Crystals of **1** consist of distorted tetrahedral, neutral molecules $[Ni^{II}(L^•)_2]$. There are two crystallographically independent sites occupied by four such molecules in the unit cell of the triclinic space group $P\bar{1}$ ($Z = 4$). The geometrical features (Figure 1) of these two independent molecules are identical within experimental error. It is clearly established that both ligands of these molecules are bound as monoanionic radicals to a nickel(II) center. The average C−N bond length of the five-membered chelates at 1.336 ± 0.01 and 1.319 ± 0.01 Å, respectively, and the av C−C bond length at 1.414 ± 0.01 Å are typical for $(L^•)^{1-}$ radicals (see above). The two best chelate planes Ni−N−C−C−N in each of the two neutral molecules in **1** form dihedral angles of 78.9° and 78.4°, respectively, which is close to the ideal tetrahedral angle of 90°.

It is remarkable that the structure of tetrahedral $[Zn^{II}(^tL^•)_2]$ in ref 2 displays very similar geometric features to those of the two identical Zn−N−C−C−N chelate rings: the av C−N bond length at 1.330 Å and the av C−C bond distance at 1.389 Å indicate again the presence of two ligand π radical monoanions.

As shown in Figure 2, crystals of **2** consist of well-separated monocations $[Ni(L^{Ox})_2]^+$ and hexafluorophosphate anions. The monocation possesses a distorted tetrahedral environment composed of two identical, crystallographically

correlated (C_2 axis), bidentate chelate rings Ni−N−C−C−N which form a dihedral angle of 70°. The av C−N distance at 1.300 ± 0.01 Å and the corresponding elongated C−C bond length at 1.461 ± 0.01 Å are indicative of the presence of two identical neutral ligands $(L^{Ox})^0$ (α-diimine) which render the central nickel ion monovalent (+I). Thus, one-electron oxidation of **1** results in an oxidatively induced reduction of the central nickel ion; eq 1 and, conversely, the reduction of **2** represents a reductively induced oxidation of the central nickel ion.

$$[Ni^{II}(L^•)_2] \equiv [Ni^I(L^{Ox})_2]^+ + e^- \qquad (1)$$
$$\textbf{(1)} \qquad\qquad \textbf{(2)}$$
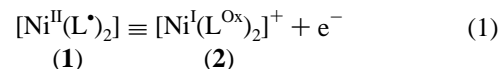
Interestingly, the structure of the monocation $[Zn^{II}(^tL^•)(^tL^{Ox})]$-(OTf) in ref 8 clearly exhibits two inequivalent ligands with differing C−N and C−C distances. The av C−N length of 1.324 Å for the first and 1.271 Å for the second ligand (C−C: 1.406 Å for the first and 1.474 Å (!) for the second) unambiguously demonstrate the presence of a neutral ligand $(^tL^{Ox})^0$ and of a single π radical anion $(^tL^•)^{1-}$. These experimental results imply that the electronic structure of the monocation in the nickel complex **2** cannot be represented as $[Ni^{II}(L^•)(L^{Ox})]^+$ with localized ligand oxidation levels $(L^•)^{1-}$ and $(L^{Ox})^0$. Due to the fact that the two five-membered chelate rings are nearly orthogonal with respect to each other, the differing oxidation levels of the two ligands, if they exist, should be localized. This is different in similar square planar nickel complexes of D_{2h} symmetry (monoanion or monocation)[41] where electron delocalization of class III prevails and the two ligands display identical C−N and C−C bond lengths that are the arithmetic mean values between those of one $(L^•)^{1-}$ and one $(L^{Ox})^0$ (or $[L^{Red}]^{2-}$).

The structure of **3** is composed of the monocation $[Ni^{II}(L^{Ox})_2(F-PF_6)]^+$ (Figure 3) and another well-separated PF_6^- anion. The cation possesses two neutral $(L^{Ox})^0$ ligands and a single F-coordinated PF_6^- anion. The Ni···F bond at 2.452(2) Å is very weak. Thus, the nickel center in the cation is five-coordinate (4 + 1), and the coordination polyhedron is best described not as square base pyramidal ($\tau = 0.0$) but trigonal bipyramidal ($\tau = 1.0$) with a τ value of 0.88 or 0.85 depending on the choice of the apical ligand (F or N21).[46] The C−N bonds of both ligands are short at av 1.280 Å, indicating the presence of C=N double bonds whereas the av C−C bond of the five-membered chelate rings is long at 1.497 Å (C−C single bond). Thus, the oxidation level of both ligands is as in $(L^{Ox})^0$ rendering the central nickel ion divalent. These ligand dimensions are very similar to those reported for $[Zn^{II}(^tL^{Ox})_2]OTf$ (av C−N 1.251 Å; C−C 1.465-(11) Å).[8] Oxidation of **2** to **3** is thus a metal-centered process.

Crystals of **4** are composed of a monocation $[Ni^{II}(L^{Ox})_2-(THF)(FPF_5)]^+$, well-separated PF_6^- anions, and an additional THF molecule of crystallization. The monocation shown in Figure 4 possesses two closed-shell neutral ligands $(L^{Ox})^0$

---

(46) τ is a geometric parameter, and it was introduced for pentacoordinated structures as a measure of trigonality. τ is 0 for a perfectly square-pyramidal geometry, while it becomes unity for a perfectly trigonal-bipyramidal geometry. Addison, A. W.; Nageswara Rao, T. *J. Chem. Soc., Dalton Trans.* **1984**, 1349.
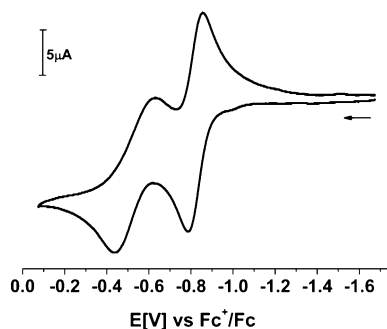
Figure 5. Cyclic voltammogram of **1** in THF at 25 °C (conditions: 0.10 M [N(*n*-Bu)₄]PF₆ supporting electrolyte; scan rate 25 mV s⁻¹; glassy carbon working electrode).

Figure 6. Electronic spectra of **1**, **2**, and **3** in CH₂Cl₂ solution at 20 °C.

Figure 7. X-Band EPR spectrum of a liquid nitrogen shock frozen CH₂-Cl₂ solution of **2** (10 K) (conditions: frequency 9.434 GHz; power 5 μW; modulation 8 G). See Table 4 for simulation parameters for the two subspectra **a** and **b**.

as is readily deduced from their C=N and C−C bond distances. The Ni···F bond at 2.318(2) Å which is shorter than its analogue in **3** despite the increase of the coordination number from five to six by binding of a sixth THF ligand in **4**.

The average Ni−N bond distance increases from **1** (1.930 Å) to **2** (1.983 Å) as one might expect for two species with the same tetrahedral polyhedron but decreasing oxidation state of the metal (+II in **1**, but +I in **2**). Upon increasing the coordination number from 4 in **1** to 5 in **3**, and to 6 in **4**, keeping the metal oxidation state constant at +II is accompanied by an increase of the av Ni−N bond length $(1.930 \rightarrow 2.009 \rightarrow 2.066 \text{ Å})$.

3. Electro- and Spectroelectrochemistry (UV−vis; EPR). The cyclic voltammogram of **1** in a tetrahydrofuran solution containing 0.10 M [N(*n*-Bu)₄]PF₆ supporting electrolyte recorded at 25 °C at a glassy carbon working electrode is shown in Figure 5. Two one-electron-transfer waves are observed at $E^1_{1/2} = -0.82$ V versus the ferrocenium/ferrocene couple (Fc⁺/Fc) and $E^2_{1/2} = -0.53$ V. From coulometric measurements it was established that both processes correspond to two successive one-electron oxidations of **1**. Interestingly, the first wave in the CV is fully reversible whereas the second wave displays a more irregularly shaped wave in accordance with the observation that one-electron oxidation of the monocation [Niᴵ(Lᴼˣ)₂]⁺ affords a cationic species [Niᴵᴵ(Lᴼˣ)₂(FPF₅)(THF)]⁺ with an increased coordination number. The process may therefore be described as an EC-mechanism (electron transfer followed by a chemical reaction). It is noteworthy that reduction of the ligands with formation of (Lᴿᵉᵈ)²⁻ is not observed in the potential range 0 to −1.7 V versus Fc⁺/Fc.

Figure 6 displays the electronic spectra of **1**, **2**, and **3** in CH₂Cl₂ solution, and Table 3 summarizes the data. We have also recorded the X-band EPR spectrum of paramagnetic **2** ($S = {}^1/_2$) in frozen CH₂Cl₂ solution at 10 K which is displayed in Figure 7.

As has been reported previously by us for a similar nickel complex, the spectrum could only be satisfactorily simulated by taking into account two subspectra, **a** and **b**. Both spectra display rather similar but not identical g_x, g_y, g_z values (Table 4). The ratio of species [**a**]/[**b**] was found to be 60:40 when the solution of **2** was shock-frozen with liquid N₂ and 45:55 in a liquid n-pentante/liquid dinitrogen bath. Upon changing
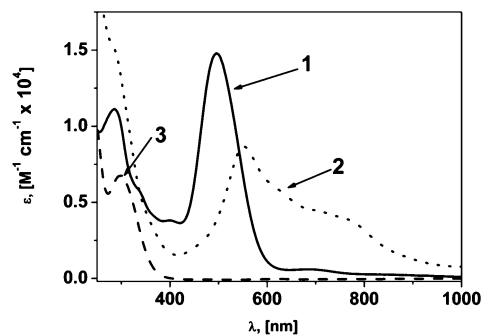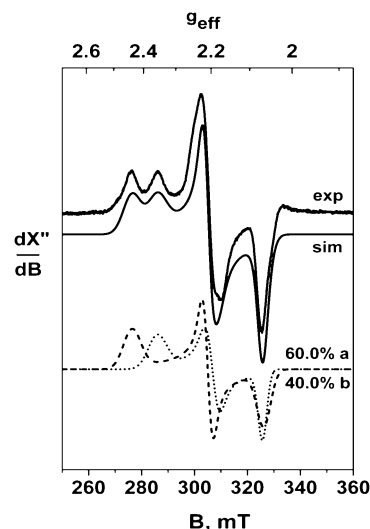
Table 3. Electronic Spectra of Complexes in CH₂Cl₂ Solution at 20 °C

complex	λ_{max}, nm (ϵ, 10^4 M⁻¹ cm⁻¹)
1	350sh, 420(0.3), 495(1.5), 700(0.08)
2	350sh, 559(0.87), 757sh(0.4), ~1800(0.2)
3	297(0.68)

Table 4. X-band EPR Spectra of **2** in Frozen CH₂Cl₂ Solution at 77 K

isomer	g_x	g_y	g_z
a	2.066	2.210	2.444
b	2.070	2.198	2.359
calcd	2.085	2.244	2.370

the freezing procedure, the [**a**]/[**b**] ratio changes indicating a thermodynamic equilibrium in solution with rapid transformation rates. It is well-established that heat transfer rates in liquid N₂ differ markedly from those in liquid n-pentane/N₂ (it is slow in the former and faster in the latter process). As noted previously, distorted tetrahedral complexes containing two asymmetric bidentate ligands exist as two geometrical isomers provided that the dihedral angle between the two five-membered chelate rings are ≠90°. In other words, the distance between the centers of the phenyl rings of the two chelates in [Ni(Lᴼˣ)₂]⁺ is different in A from that in B.

We note that the g-anisotropy of the paramagnetic monocations **a** and **b** in solution of **2** is quite large. This is interpreted as a clear indication that the unpaired electron

A   or   B
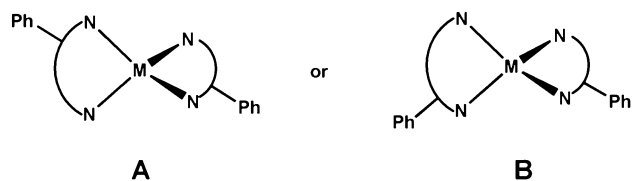
resides in Ni d-orbital rather than in a π^* ligand orbital. Thus, two electron configurations must be considered: (a) a genuine Ni(I) complex with a d^9 electron configuration as in distorted tetrahedral $[Ni^I(L^{Ox})_2]^+$ containing two closed-shell 1,2-diimine ligands $(L^{Ox})^0$ or (b) a nickel(II) complex with a d^8 electron configuration $(S_{Ni} = 1)$ and a single localized or delocalized ligand π radical monoanion $[Ni^{II}(L^{\bullet})$-$(L^{Ox})]^+ \leftrightarrow [Ni^{II}(L^{Ox})(L^{\bullet})]^+$ where the ligand spin $(S_{rad} = {}^1/_2)$ couples intramolecularly antiferromagnetically with the nickel ion $(S_{Ni} = 1)$ yielding the observed $S = {}^1/_2$ ground state. The present EPR spectra alone do not allow to unequivocally distinguish between choices a and b.

4. DFT Calculations. a. Optimized Geometries. Here we first develop a detailed picture of the electronic structures of the zinc complexes $[Zn^{II}(^tL^{\bullet})_2]$, $[Zn^{II}(^tL^{Ox})(^tL^{\bullet})]^+$, $[Zn(^tL^{Ox})_2]^{2+}$, and $[Zn^{II}(^tL^{\bullet})(^tL^{Red})]^-$ and then of the nickel complexes $[Ni^{II}$-$(L^{\bullet})_2]$, $[Ni^I(L^{Ox})_2]^+$, and $[Ni^{II}(L^{Ox})_2]^{2+}$. As pointed out above, the molecular structures of **5**, **6**, and **8**, and of **1**, **2**, and **3** have been determined by X-ray crystallography at cryogenic temperatures.

The geometry of **5** was optimized under the assumptions of either an $S = 1$ state or a broken-symmetry BS(1,1) antiferromagnetically coupled singlet state with the B3LYP functional. The two structures were found to be essentially identical and within the scatter of the relaxation procedure also of identical energy (e.g., within 0.1 kcal/mol). Thus, we conclude that there are two unpaired electrons in **5** that are essentially uncoupled. Examination of the spin-density profiles indicates that the two unpaired electrons are situated on the ligands that are thus in a π-radical state. Interestingly, the calculated C−N and C−C bond lengths in all three states are identical (see Figure 8) and in excellent agreement with experiment. These data support the presence of two π-radicals in **5**. The calculated av Zn−N bond lengths are overestimated by ~0.05 Å, a result which is typical for the B3LYP functional. The calculated dihedral angle between the two metallacycles at 80.2° is also in excellent agreement with experiment.

For neutral $[Ni(L^{\bullet})_2]$ (**1**), the ground state geometry was calculated for a BS(2,2) $M_s = 0$ state. In this instance, a stationary state on the potential energy surface was located where the calculated bond distances within the two equivalent ligands are in excellent agreement with experiment and indicative of the presence of two ligand π radicals $(L^{\bullet})^{1-}$. The Ni−N distances are again overestimated by ~0.08 Å. We also calculated a closed-shell $S = 0$ state and a high-spin, open-shell $S = 2$ state for **1** which were both found to be higher in energy by 15.7 and 16.0 kcal mol^{-1}, respectively, than the BS (2,2) $M_s = 0$ state. We refrain from a discussion of these solutions. In summary, the present geometry optimizations shown in Figure 8 for **1** and **5** are in excellent accord with experiment and indicate the presence of two
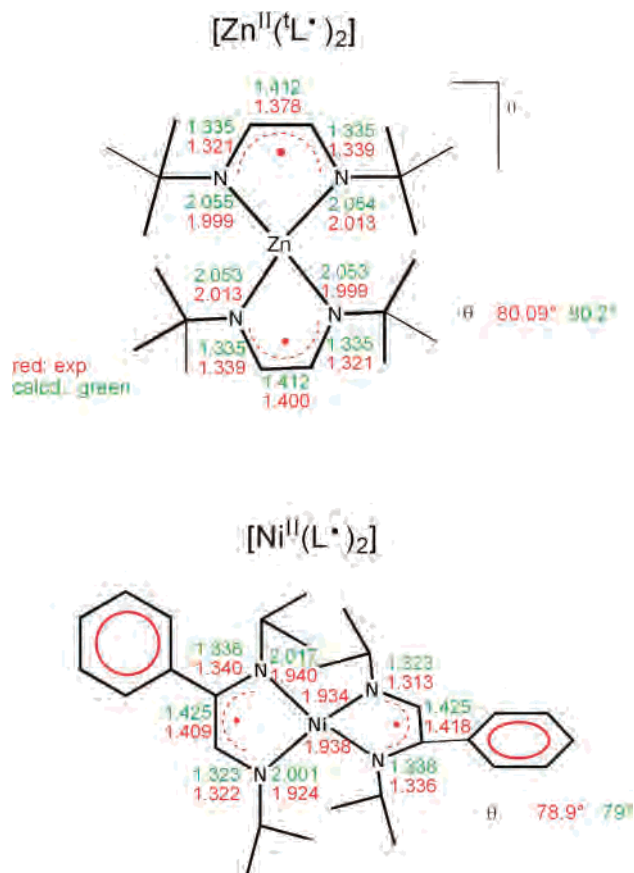
Figure 8. Experimental (red) and calculated (green) lengths (Å) in **5** (top) and **1** (bottom).

ligand π radical monoanions and a Zn(II) $(S_{Zn} = 0)$ and a Ni(II) $(S_{Ni} = 1)$, respectively.

In a very similar fashion, we have calculated and optimized the geometry of the monocations in **6** and **2**. Attempts to find broken symmetry solutions BS(2,1) for **2** and BS(1,0) for **6** failed. In both cases, the $S = {}^1/_2$ solution was found only. Thus, attempts to calculate $[Ni^{II}(L^{\bullet})(L^{Ox})]^+$ with a high-spin Ni(II) ion and an antiferromagnetically coupled ligand radical $(L^{\bullet})^{1-}$ reverted to the $S = {}^1/_2$ (Ni(I), d^9) solution (see below). The results are shown in Figure 9. The calculated structure of the monocation in **6** indicates the presence of two different ligands, namely a π radical monoanion $(^tL^{\bullet})^{1-}$ and a neutral ligand $(^tL^{Ox})^0$. The C−N and C−C distances are different in both ligands. They agree very well with the experimental data. Thus, **6** clearly contains a cation $[Zn^{II}$-$(^tL^{Ox})(^tL^{\bullet})]^+$ where the unpaired electron is localized on one monoanion $(^tL^{\bullet})^{1-}$. In stark contrast, the structure of the cation in **2** contains two equivalent ligands with four short C−N bonds (1.29 Å) and two long C−C bond lengths at 1.47 Å which correspond to C=N double and C−C single bonds, respectively, rendering the oxidation level of both ligands $(L^{Ox})^0$. Consequently, the oxidation state of the central nickel ion must be +I. These calculated data are again in excellent agreement with experiment.

The optimized geometry of the diamagnetic, closed-shell dication $[Zn(^tL^{Ox})_2]^{2+}$ (**7**) $S = 0$ is shown in Figure 10. The agreement between experiment[8] and calculation is only reasonable due to the low quality of the X-ray structure of
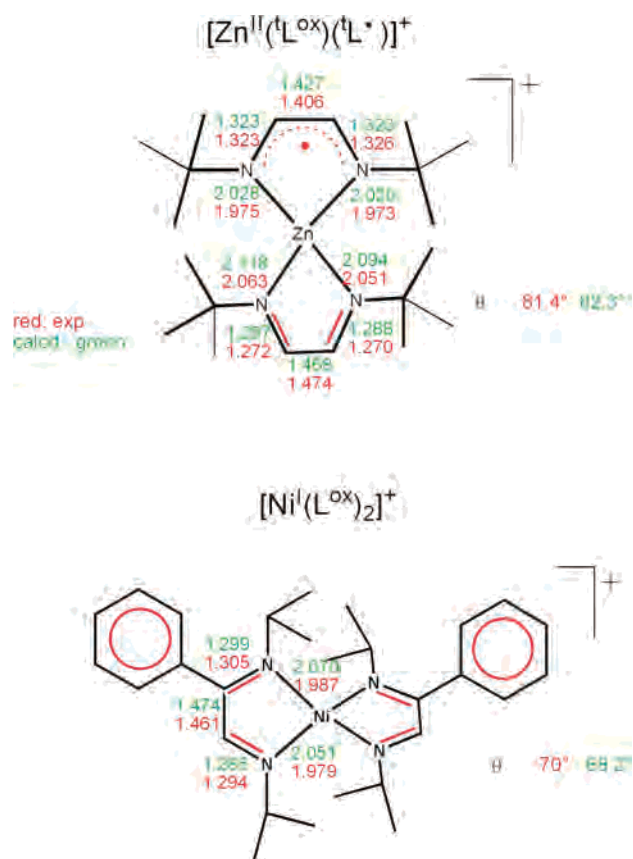
Figure 9. Experimental (red) and calculated (green) bond lengths (Å) in the monocations of **6** (top) and **2** (bottom). θ represents the dihedral angle between the two M−N−C−C−N chelate rings.

Figure 10. Experimental (red) and calculated (green) bond lengths (Å) in the dication $[Zn^{II}(^{t}L^{Ox})_2]^{2+}$ in **7** (top) and hypothetical $[Ni^{II}(L^{Ox})_2]^{2+}$ ($S = 1$) (bottom). The experimental data for the latter were taken from the crystal structure of **3**.

Figure 11. Experimental (red) and calculated (green) bond lengths (Å) in the monoanion $[Zn^{II}(^{t}L^{Red})(^{t}L^{\bullet})]^{-}$.

7, but it is nonetheless unambiguously established that the ligands are at the $(^{t}L^{Ox})^0$ oxidation level. Similarly, the calculations of the hypothetical, paramagnetic dication $[Ni^{II}-(L^{Ox})_2]^{2+}$ ($S = 1$) show the presence of the two neutral $(L^{Ox})^0$ ligands. The C−N and C−C distances are in excellent agreement with those measured in **3** containing the five-coordinate monocation $[Ni^{II}(L^{Ox})_2(FPF_5)]^+$ and **4** with a six-coordinate monocation $[Ni^{II}(L^{Ox})_2(THF)(FPF_5)]^+$.

Finally, we have optimized the geometry of the paramagnetic monoanion $[Zn^{II}(^{t}L^{Red})(^{t}L^{\bullet})]^{-}$ ($S = ^1/_2$). The results are shown in Figure 11 where it is clearly seen that the two ligands exist in two different, localized oxidation levels, namely $(^{t}L^{Red})^{2-}$ and $(^{t}L^{\bullet})^{1-}$. This result is in excellent agreement with experiment[8] and calculations for neutral $[Al^{III}(^{t}L^{Red})(^{t}L^{\bullet})]$ in ref 13.

b. Electronic Structures. A qualitative bonding scheme derived from the spin-unrestricted BS calculation of **1** is shown in Figure 12. Five orbitals which are mainly of metal d character are identified. Three of these orbitals are found in the spin-up and the spin-down manifolds; they are doubly occupied. The other two nickel-based orbitals originate from the t_2 set and occur only in the spin-up manifold. These two orbitals are thus singly occupied with parallel spins. This pattern defines a high-spin Ni(II) configuration ($S_{Ni} = 1$) at the metal center. In addition to these two metal-centered SOMOs, two ligand-centered orbitals are identified in the spin-down manifold which are not populated in the spin-up manifold, thus leading to the observed overall $M_s = 0$ BS
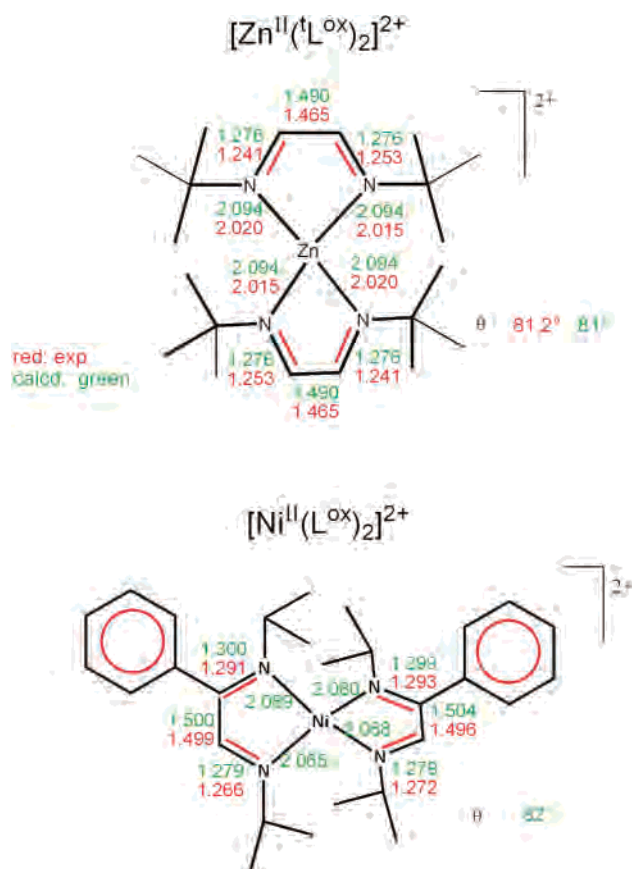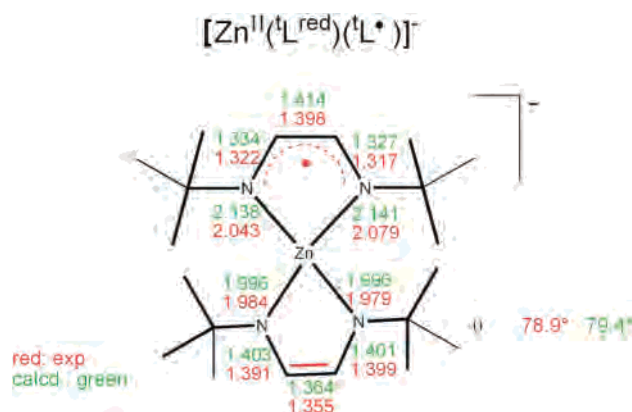
state. These orbitals correspond to two symmetry-adapted combinations of the SOMO of the two ligand radicals. Thus, the basic electronic structure description of **1** features a high-spin Ni(II) ion which is strongly antiferromagnetically coupled to two ligand-centered π radicals.[24,25] The calculated spatial overlaps for these corresponding metal−ligand couples are at $S = 0.54$ and 0.52, indicative of the antiferromagnetic nature of these interactions. The magnetic exchange coupling constant J was calculated to be -1250 cm^{-1} according to the Yamaguchi approach[47] ($\hat{H}_{HDvV} = -2J\hat{S}_A \cdot \hat{S}_B$). This calculated large value is in accord with the experimental
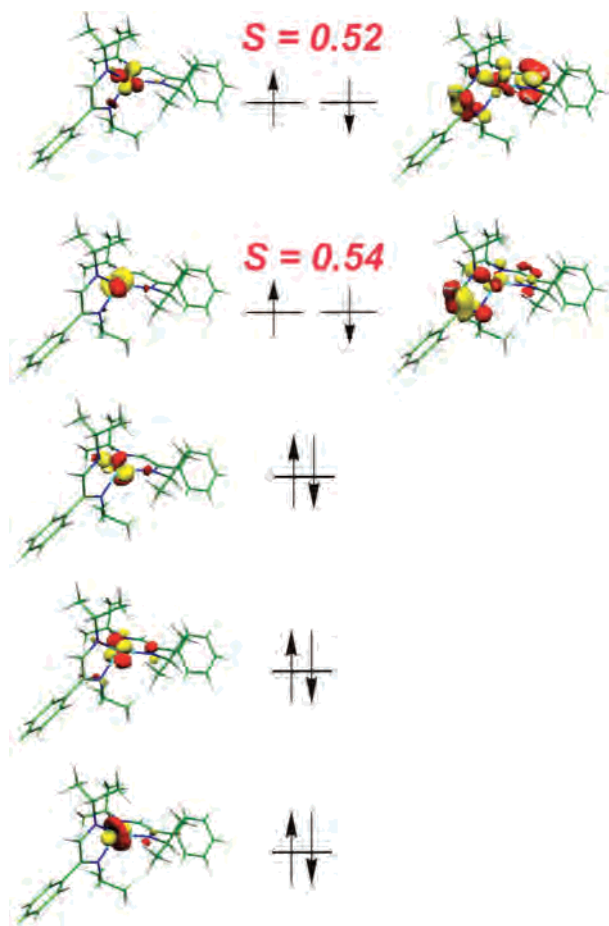
Figure 12. Qualitative MO diagram of the corresponding orbitals[35] of magnetic pairs of **1** as derived from the broken symmetry DFT calculations (B3LYP).
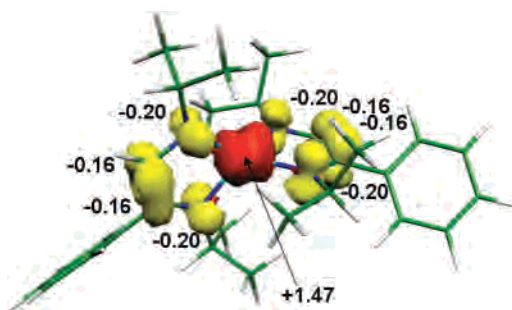

Figure 14. Spin density plot of **5** as derived from (a) $S = 1$ (left) and (b) $S = 0$ (right) DFT calculations.

Figure 15. Spin density plot of the monocation $[Zn^{II}(^{t}L^{Ox})(^{t}L^{\bullet})]^{+}$ in **6** ($S = 1/2$) as derived from DFT calculations.

Figure 13. Spin density plot of **1** as derived from BS DFT calculations together with values of the spin density of the Mulliken spin population analysis.

finding that **1** possesses a singlet ground state up to 20 °C with no indication of thermal population of higher spin states.

Keeping in mind the caveats pointed out in refs 24 and 25, it is possible to analyze the spin density in **1**. The corresponding plot for **1** is shown in Figure 13 which nicely visualizes the antiparallel spin alignment between the high-spin Ni(II) (positive spin density in red) and the radical ligands (negative spin density in yellow). An approximate

(47) (a) Soda, T.; Kitagawa, Y.; Onishi, T.; Takano, Y.; Shigeta, Y.; Nagao, H.; Yoshioka, Y.; Yamaguchi, K. *Chem. Phys. Lett.* **2000**, *319*, 223. (b) Yamaguchi, K.; Takahara, Y.; Fueno, T. In *Applied Quantum Chemistry*; Smith, V. H., Eds.; Reidel: Dordrecht, 1986; p 155.
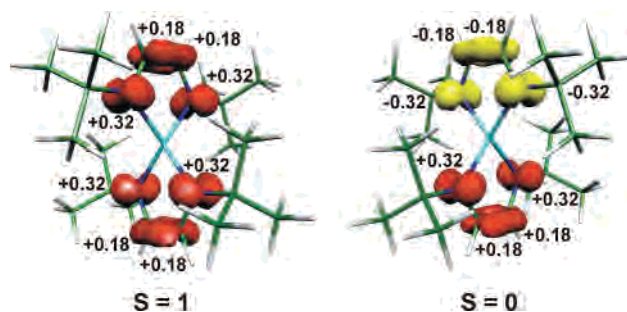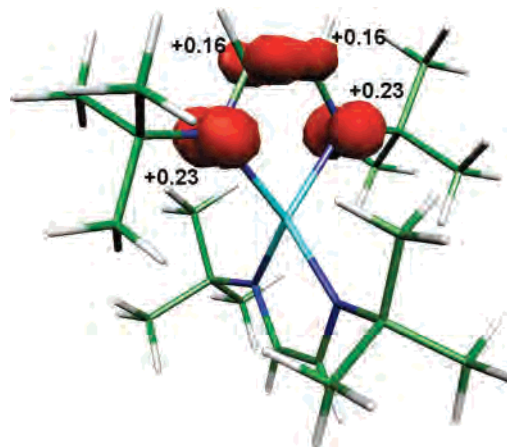(48) Löwdin, P.-O. *Adv. Quantum Chem.* **1970**, *5*, 185.

breakdown of the spin density into atomic contributions via a spin population analysis supports the presence of two unpaired electrons at the Ni ion with positive spin and two unpaired electrons with negative spin localized on both ligand π radicals.

It is now very instructive to compare these results with those obtained for the analogous zinc complex **5**. Five predominantly metal d orbitals which are each doubly occupied were identified indicating the presence of a Zn(II) ion (d^{10}, $S_{Zn} = 0$). In addition, two singly occupied ligand-based π orbitals are identified which possess parallel spin orientation in the $S = 1$ state but are antiparallel in the $S = 0$ state as shown in the spin density plot of Figure 14. Since the singlet and triplet states are nearly degenerate, the two spins in **5** are essentially uncoupled.

It is now very interesting that for the monocation $[Zn^{II}(^{t}L^{\bullet})(^{t}L^{Ox})]^{+}$ in **6** we identify again five doubly occupied metal d orbitals as expected for a Zn(II) ion (d^{10}, $S_{Zn} = 0$) and, in addition, one singly occupied orbital at the ligand π radical $(^{t}L^{\bullet})^{1-}$. The spin density plot shown in Figure 15 clearly establishes that only this ligand orbital carries spin density. The ligand $(^{t}L^{Ox})^{0}$ is a closed-shell, neutral ligand without spin density ($S_{L}^{Ox} = 0$).

In stark contrast is the calculated electronic structure of the corresponding monocation $[Ni^{I}(L^{Ox})_{2}]^{+}$ in **2**. As displayed in Figure 16a, five predominantly metal d orbitals are clearly identified, the first four of which are doubly occupied whereas the fifth d-orbital is only singly occupied. This is indicative of the presence of a paramagnetic Ni(I) ion (d^{9};
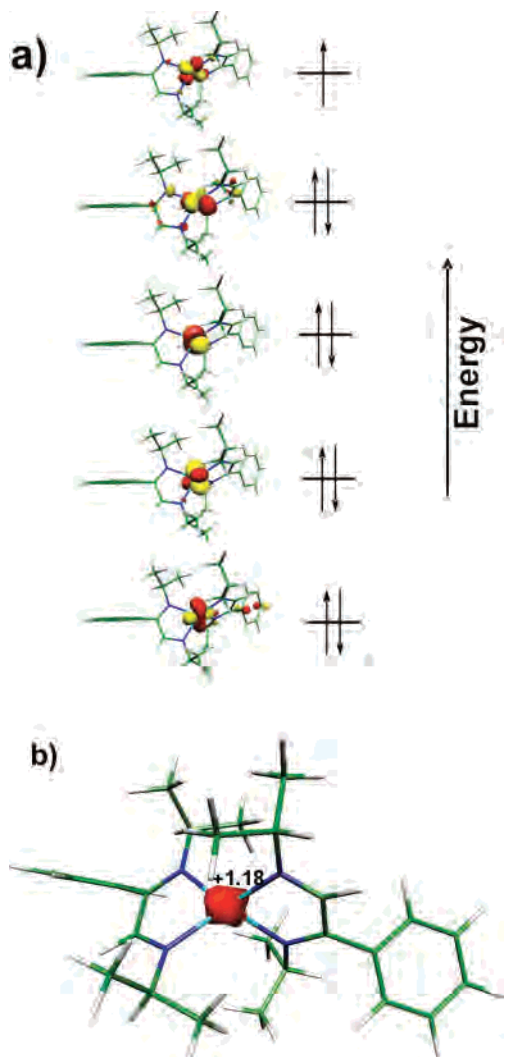
Figure 16. (a) Qualitative MO diagram of the corresponding orbitals of **2** as derived from DFT calculations. (b) Spin density plot of the monocation in **2** ($S = \frac{1}{2}$).

$S_{Ni} = \frac{1}{2}$). All ligand orbitals are either doubly or not occupied at all as is expected for two closed-shell diamagnetic $(L^{Ox})^0$ ligands. Accordingly, the spin density shown in Figure 16b is localized at the nickel center; no spin density is observed on the ligands. Thus, the electronic structures of the monocations of Zn in **6** and of nickel in **2** are very different: $[Zn^{II}(^tL^{\bullet})(^tL^{Ox})]^+$ versus $[Ni^I(L^{Ox})_2]^+$.

Finally, the hypothetical tetrahedral dication $[Ni^{II}(L^{Ox})_2]^{2+}$ contains five predominantly metal d orbitals, the first three of which are doubly occupied whereas the remaining two d orbitals are only singly occupied. This is representative for a paramagnetic Ni(II) ion (d^8, $S_{Ni} = 1$) in a tetrahedral ligand environment composed of two neutral (L^{Ox}) ligands.

For the sake of completeness, the electronic structure of the monoanion $[Zn^{II}(^tL^{Red})(^tL^{\bullet})]^-$ is best described as a Zn(II) ion (d^{10}, $S_{Zn} = 0$) coordinated to a diamaganetic dianion

$(^tL^{Red})^{2-}$ and a paramagnetic monoanion $(^tL^{\bullet})^{1-}$ ($S_{Rad} = \frac{1}{2}$). The ligand centered radical is localized at the one $(^tL^{\bullet})^{1-}$ ligand.

Conclusions

Three members of the electron-transfer series $[Ni(L)_2]^z$ ($z = 0, 1+, 2+$) have been synthesized and structurally and spectroscopically characterized (UV−vis, EPR, electro- and magnetochemically). In addition, broken symmetry DFT calculations have been performed for each member in order to elucidate their electronic structures. The computational methodology employed has been calibrated by calculations of the corresponding series $[Zn^{II}(^tL)_2]^z$ ($z = 2+, 1+, 0, 1-$) where the results were found to be in excellent agreement with experiment in ref 8. The most salient results of this work may be summarized as follows.

(a) The tetrahedral, neutral complexes $[Ni^{II}(L^{\bullet})_2]$ and $[Zn^{II}(^tL^{\bullet})_2]$ contain both a divalent metal ion and two monoanionic α-diimine ligand π radicals. In the diamagnetic nickel(II) complex, the central high spin metal ion ($S_{Ni} = 1$) is strongly antiferromagnetically coupled to two ligand π radicals ($S_{rad} = \frac{1}{2}$) yielding an $S_t = 0$ ground state. In contrast, the tetrahedral Zn complex ($S_{Zn} = 0$) contains two essentially uncoupled π radical ligand anions which render this species paramagnetic.

(b) One-electron oxidation of the neutral species yields the tetrahedral monocations: $[Ni^I(L^{Ox})_2]^+$ and $[Zn^{II}(^tL^{Ox})$-$(^tL^{\bullet})]^+$ both with an $S_t = \frac{1}{2}$ ground state but with differing electronic structures. The nickel complex contains a central Ni(I) ion (d^9, $S_{Ni} = \frac{1}{2}$) and two neutral α-diimine ligands L^{Ox}. Thus, the electrochemical or chemical one-electron oxidation of the neutral complex $[Ni^{II}(L^{\bullet})_2]$ involves oxidation of both ligand radicals (one electron goes to the oxidant and one to the Ni(II) ion) and a one-electron reduction of the Ni(II) ion. In contrast, the zinc monocation $[Zn^{II}(^tL^{Ox})(^tL^{\bullet})]^+$ consists of a diamagnetic Zn(II) ion (d^{10}, $S_{Zn} = 0$), one anionic ligand π radical $(^tL^{\bullet})^{1-}$, and one neutral oxidized α-diimine ligand $(^tL^{Ox})$ yielding an $S_{rad} = S_t = \frac{1}{2}$ ground state.

(c) The tetrahedral dications $[Ni(L^{Ox})_2]^{2+}$ and $[Zn^{II}(^tL^{Ox})_2]^{2+}$ consist of a central Ni(II) ion ($S_{Ni} = 1$) and a diamagnetic Zn(II) ion (d^{10}, $S_{Zn} = 0$) and two neutral, diamagnetic α-diimine ligands, respectively.